Structural Brain Mapping Using Antibody-Conjugated Gold Nanoparticles and X-ray Microscopy

by

Logan Thrasher Collins

Department of Psychology and Neuroscience; University of Colorado at Boulder

Thesis advisor:

Dr. Michael Saddoris; Department of Psychology and Neuroscience

Defense committee:

Dr. Michael Saddoris; Department of Psychology and Neuroscience

Dr. Andreas Hoenger; Department of Molecular, Cellular, and Developmental Biology

Dr. Heidi Day; Department of Psychology and Neuroscience

Abstract

The current gold standard in cellular connectomics uses serial section electron microscopy approaches. But even when mapping very small regions of neural tissue (i.e. hundreds of micrometers), electron microscopy techniques can take months or years of work. Nondestructive methods which employ x-ray microscopy may facilitate far more efficient connectomic at resolutions sufficient for visualizing dendrites and axons. However, x-ray microscopy has so far been limited by chemical stains that cannot target desired tissue structures. A potential way of moving past this limitation is to use a gold nanoparticle contrast agent with covalently linked antibodies. To this end, an anti-dopamine 1 receptor antibody (anti-D1R) was conjugated to 60×27 nm gold nanorods. Immunohistochemical assays were performed on sections of rat striatum to verify the staining efficacy of these immunogold constructs. After an anti-Fab secondary antibody linked to Alexa Fluor® 488 was reacted with the primary antibodies on the gold nanorods, tissue fluorescence demonstrated that the immunogold had bound the striatum. X-ray microscopy was performed using a ZEISS Xradia 520 Versa x-ray microscope on a region of striatum that had been treated with the immunogold contrast agent. With a scan time of just 13h, the resulting three-dimensional reconstruction revealed neurites at a 386 nm pixel size. Next, a thick tissue volume was treated using 5 nm spherical gold nanoparticles with covalently linked anti-D1R antibodies. This volume was then imaged via x-ray microscopy at a pixel size of 403 nm and with a scan time of 16h. Some neurites were visible in the reconstruction, but the high concentration of nanoparticles may have obscured many of the finer features. The proof-of-concept data acquired from rat striatum demonstrate this approach's promise for high-throughput imaging of neuronal tissue.

Introduction

There is an increasing trend in computational neuroscience towards creating predictive models of brain function using biophysically detailed networks of *in silico* neurons (Bezaire, Raikov, Burk, Vyas, & Soltesz, 2016; Markram, 2006; Markram et al., 2015; Oberlaender et al., 2011). These networks are often composed of multicompartmental Hodgkin-Huxley-type models, a class of virtual neuron that incorporates the anatomy of the dendritic arbor into its electrophysiological modeling. Multicompartmental simulations provide a powerful tool for realistically describing nonlinear voltage propagation across neuronal membranes as well as producing realistic spiking activity (Novère, 2012). However, the connectivity of the networks involved in these computational studies tends to result from rough probabilistic measures of biological connectivity (Bezaire et al., 2016; Egger, Dercksen, Udvary, Hege, & Oberlaender, 2014; Markram et al., 2015; Oberlaender et al., 2011). For instance, Markram et al. used data on the average connectivity patterns among different cell types for algorithmically generating networks to model rat cortical columns. Although useful for predicting mesoscale emergent phenomena such as oscillations, this form of statistical connectivity does not capture the specific wiring that is required to perform many brain functions. The reason behind using statistical connectivity patterns rather than exact wiring arises from a lack of methods for rapidly reconstructing large volumes of neuronal tissue at sufficient resolution to observe subcellular structures like axons and dendrites.

The current leading techniques in connectomics are serial section electron microscopy (ssEM) and approaches that combine expansion microscopy (ExM) with standard light-sheet fluorescence microscopy (LSFM) or lattice light-sheet microscopy (LLSM). Techniques that use ssEM allow very high resolution (i.e. often with less than 10 nm pixel sizes) brain imaging by passing an electron beam through a series of very thin tissue sections (Takemura et al., 2017). However, ssEM

can take months or years to image tissue volumes with submillimeter dimensions (Schalek et al., 2016; Wanner, Kirschmann, & Genoud, 2015). Light-sheet fluorescence expansion microscopy (LSFEM) and expansion lattice light-sheet microscopy (ExLLSM) employ ExM along with LSFM and LLSM respectively. ExM facilitates isotropic enlargement of tissue samples via infusion of a swellable polymer network and so allows for super-resolution imaging with conventional microscopes (F. Chen, Tillberg, & Boyden, 2015). In addition, expanded samples take on a degree of optical translucency which is useful for three-dimensional imaging. LSFM uses a cylindrical lens to create a planar light sheet that can be swept through a sample for three-dimensional reconstruction (Power & Huisken, 2017). LLSM is a special form of LSFM that employs a spatial light modulator to create light sheets from Bessel beams and two-dimensional optical lattices (Chen et al., 2014). Bürgers et al. used LSFEM image volumes of mouse hippocampus at 135×135×590 nm resolution. The largest of these volumes had post-expansion dimensions of 3,600×1,240×275 μm. To create the final reconstruction, 70 z-stacks were stitched together. Gao et al. employed ExLLSM to create detailed three-dimensional reconstructions of all dopaminergic neurons and all presynaptic boutons within a 1,400×2,700×370 μm volume that covered the entire post-expanded *Drosophila* brain (Gao et al., 2019). Because of the specialized LLSM optics used in the study, the resolution of the dataset was 60×60×90 nm. However, ExLLSM is limited by its 160 μm field of view (FOV) and 1.5 mm scan range even when using a specially designed lattice light-sheet microscope optimized for ExM. As a result, reconstructing the *Drosophila* brain required stitching of thousands of image tiles. Although ssEM, LSFEM, and ExLLSM provide advantages in resolution, they would not be practical for working with pre-expansion samples much larger than 1 mm^3.

Tissue clearing is another method often used for imaging three-dimensional tissue structures. In tissue clearing, a sample is chemically treated to render it optically translucent (Du, Hou, Zhang, & Li, 2018). But with the exception of ExM (which is often considered a clearing technique itself due to the optical translucency that results from the expansion process), tissue clearing techniques do not allow for imaging of large volumes at high resolutions. With cleared tissue, resolution and FOV is limited by the optics used for imaging. Large volumes such as whole cleared mouse brains can be imaged at low resolution using LSFM setups (Qi et al., 2019) or small volumes can be imaged at high resolution using super-resolution microscopy (Ke et al., 2016). But achieving both high resolution and large volume imaging without enormously extending the acquisition time remains out of reach.

X-ray microscopy (XRM) represents a powerful and largely unexploited tool for structural connectomics. XRM involves staining tissue samples with high-z contrast agents, rotating the samples while exposing it to x-rays, and computationally reconstructing three-dimensional images. The high electron density of the contrast agents acts to absorb the x-rays. Although XRM has a lower resolution than ssEM, LSFEM, and ExLLSM, XRM still exhibits sufficient resolution to visualize the detailed morphologies of neurons (Fonseca et al., 2018; Mizutani, Saiga, Takeuchi, Uesugi, & Suzuki, 2013; Mizutani et al., 2011). XRM is nondestructive, works on timescales of minutes to hours, and needs less computational resources than ssEM for three-dimensional reconstruction (Mizutani et al., 2016). XRM may eventually provide a platform for rapid imaging and reconstruction of connectomes over volumes that greatly exceed 1 mm^3.

As mentioned, high-z contrast agents are required to visualize neuronal tissue with x-ray microscopy. Many investigators have employed chemical stains for this purpose. Mizutani et al. used the BL47XU beamline of the SPring-8 synchrotron facility to make a rough wiring diagram

of a 220×328×314 μm volume encompassing an entire *Drosophila* brain hemisphere at an estimated spatial resolution of 0.6-0.8 μm^3 (Mizutani et al., 2013). For x-ray contrast, a modified reduced silver impregnation protocol was utilized. The FOV was 524×524×183 μm and four three-dimensional image tiles were stitched together to make the final reconstruction. The imaging process took place over a time period of 64 minutes (16 minutes per tile). In a study by Fonseca et al., XRM was used to reconstruct the three-dimensional morphologies of a sparse subset of neurons within 2.4 mm^3 volumes of mouse hippocampal and cortical tissue (Fonseca et al., 2018). To do this, a Golgi-Cox staining protocol was employed to grant x-ray contrast to a subset (around 3-10%) of neurons within the volume. The tissue was then imaged using the UVX-LNLS synchrotron's IMX beamline. The voxel size was 0.82 μm^3, the acquisition time was 40 minutes, and the entire volume was captured in a single acquisition. At this resolution, neurites and even the rough locations of some dendritic spines were visible in the reconstructions. Furthermore, the neurons were clear enough to undergo manual segmentation. XRM has also been used for imaging whole larval and juvenile zebrafish at 0.743 μm^3 and 1.43 μm^3 voxel size respectively (Ding et al., 2019). Phosphotungstic acid (PTA) acted as the x-ray contrast agent for staining the zebrafish. Only 2-5 acquisitions were necessary for imaging each zebrafish due to the 1.5 mm^3 FOV for the larval specimens and the 3.0 mm^3 FOV for the juvenile specimens. A polychromatic pink beam allowed for each acquisition to take place over a time period of just 20 seconds. Some other examples of chemical contrast agents for soft tissue include osmium tetroxide, gold reagents, and iodine reagents (Metscher, 2009; Mizutani & Suzuki, 2012). However, most contrast agents accumulate more or less randomly and do not possess the ability to target desired cells or subcellular structures within tissue. To the best of my knowledge, only one targeted stain has been applied towards imaging brain tissue via x-ray microscopy (Mizutani, Takeuchi, Akamatsu,

Uesugi, & Suzuki, 2008). Mizutani et al. used colloidal gold to selectively stain *Drosophila*'s optic lobe cortex. However, this only revealed structure at the tissue scale and no morphology at the cellular or subcellular scale was visible.

Here, I develop a contrast agent consisting of gold nanoparticles with covalently linked antibodies for x-ray microscopic visualization of targeted structures within brain tissue. In this case, anti-D1R antibodies are used to target the nanoparticles to D1R-expressing neurons within rat striatum. I show that this technique can provide sufficient resolution to observe neurites and cell bodies. I demonstrate acquisition of large three-dimensional reconstructions with rapid scan times using a ZEISS Xradia 520 Versa laboratory XRM. The first reconstruction was performed over 13h with an ~0.7 mm^3 FOV and a 386 nm pixel size and the second reconstruction was performed over 16h with an ~0.8 mm^3 FOV and a 403 nm pixel size. It should be noted that similar results could most likely be achieved much more rapidly (on the order of a few minutes or less) using a synchrotron source. I illustrate that immunogold-based x-ray microscopy holds promise for studies of three-dimensional tissue ultrastructure and connectomics.

This research uses the striatal D1R as a molecular target of interest for x-ray microscopy. In the striatum, D1R is expressed on the plasma membranes of medium spiny neurons (MSNs), a type of GABAergic cell which projects to the basal ganglia to help shape motor outputs, reward learning, and habit formation. Due to these projections, MSNs represent an important part of the pathways implicated in addiction. Furthermore, MSNs comprise about 95% of the cells in the striatum (Matamales et al., 2009). D1R is a G-protein coupled receptor and its activation by dopamine leads to stimulation of MSN activity via signaling pathways which modulate both voltage-gated and ligand-gated ion channels. (Surmeier, Ding, Day, Wang, & Shen, 2007). Because of its central role in the modulation of MSNs, D1R is a vital part of striatal circuitry.

Deciphering the microanatomy of the striatum may facilitate creation of a three-dimensional anatomical reference atlas for the area at a subcellular scale. Although this study only images small parts of the striatum, it represents a first step towards the goal of imaging the entire region. Acquiring x-ray reconstructions of the healthy striatum and diseased striatum (e.g. from animals with drug addiction) may reveal ultrastructural differences with potential clinical relevance. Tagging desired biomarkers with immunogold may enable exploration of the three-dimensional distribution of molecules of interest within the healthy and diseased striatum. This may open numerous possibilities for using x-ray microscopy to help understand how the striatum operates in both healthy and dysfunctional states.

In the long term, using x-ray microscopy and immunogold as a tool for connectomics could help advance a computational systems biology approach to neuroscience. By coupling morphological and connectivity data to large-scale multicompartmental Hodgkin-Huxley simulations (Arkhipov et al., 2018; Bezaire et al., 2016; Markram et al., 2015), the mechanistic operations of neural circuits could be deciphered *in silico* with a level of precision and throughput that vastly exceeds any purely experimental effort. While experimental comparison would still be vital for refining and verifying these models, the simulations would rapidly generate probable mechanisms which could allow for much more efficient use of experimental resources. Furthermore, large-scale simulations will likely prove crucial for systems-level understanding of brain function (Einevoll et al., 2019). If the brain is a puzzle, current neuroscientific efforts attempt to glean insight from one or two pieces at time without ever putting together more than a tiny fraction of the whole. The rapid imaging capabilities of x-ray microscopy combined with the molecular specificity of nanoparticle-based labeling techniques may pave the way towards acquiring sufficient data to create biologically realistic simulations of brain tissue and eventually

entire brains. Achieving such a goal would be like putting together the whole puzzle, allowing investigation of the complete system.

Although whole-brain simulation is still fairly distant, this study takes some early steps towards devising an imaging pipeline that may enable such a lofty aim. As previously described, synchrotron-based x-ray microscopy allows extremely rapid imaging of neuronal tissue (Ding et al., 2019; Fonseca et al., 2018; Hwu, Margaritondo, & Chiang, 2017; Mizutani et al., 2013). In many cases, the resolution is high enough to resolve axons and dendrites, but not high enough to identify synapses. Nanoparticle-based labeling of synapses within x-ray microscopic reconstructions could allow dense mapping of neuronal connectivity without ssEM. Other biomarkers (e.g. dopamine receptors as in this study) could undergo nanoparticle tagging to further interrogate molecular functionality in the context of structure. As such, this investigation lays the groundwork for rapidly imaging the molecular properties of neuronal tissue via x-ray microscopy.

Results

Prior to performing x-ray microscopy, 40 μm slices of rat striatum were imaged using fluorescence microscopy as a quality control measure. After conjugating anti-D1R antibodies to 60×27 nm gold nanorods, the resulting constructs were used to carry out immunohistochemical assays on the 40 μm striatal slices (with a 1:100 dilution from the immunogold stock). As a control, 40 μm slices from the rat striatum were treated by 60×27 nm gold nanorods without conjugated antibodies (also using a 1:100 dilution from the stock solution). Both samples were reacted with an anti-Fab secondary antibody linked to Alexa Fluor® 488 (Fig. 1A). Fluorescence microscopy was employed to determine whether the immunogold constructs had successfully adhered to the tissue. Striatum samples treated with anti-D1R immunogold demonstrated visible fluorescence on

the fluorescence microscope's Alexa Fluor® 488 channel (Fig. 1B). As expected for the D1R antigen, fluorescent patches were localized to cell membranes. By comparison, the tissue treated with unmodified nanorods did not exhibit Alexa Fluor® 488 fluorescence (Fig. 1C). This experimental process illustrated that the immunogold is capable of selectively binding its target antigen within the tissue.

The ZEISS Xradia 520 Versa XRM was employed to acquire three-dimensional images of the 40 μm slices. The slices were removed from their slides and placed inside of 1 mm diameter plastic tubes. To minimize desiccation, the tubes were sealed with rubber plugs. The immunogold-treated sample underwent a 13h scan (3,000 projections) with a ~0.7 mm^3 FOV using the XRM's 20x lens. The three-dimensional reconstruction reveals the sample's cellular ultrastructure (Fig. 2A,B). Branching filaments are clearly visible throughout the reconstructed region, demonstrating that this technique can resolve dendrites and axons. In addition, globular extensions can be seen on many of the filaments. Based on their sizes, these extensions might correspond to dendritic spines. The reconstruction also includes a well-delineated cell that is identifiable as a MSN (Fig. 2C) as well as a pair of long filaments that might be axons. These data illustrate the utility of the immunogold stain for XRM-mediated visualization of neuronal tissue.

The control sample (treated with unmodified nanorods) was subjected to a 4.5h scan (800 projections) with a ~0.7 mm^3 FOV using the XRM's 20x lens. Fewer projections were used for the control because of the instrument's limited availability. Using fewer projections should not impact the overall result as the main benefit of using more projections is to minimize minor aberrations in the image. In the control sample, only the rough shape of the tissue is visible (Fig. 3A,B). Scattered regions of higher absorbance could be seen, but they were not ascribable to any

sort of morphological feature. This outcome demonstrates that the conjugated antibodies were vital to the ability of the gold nanoparticles to act as an x-ray contrast agent.

A computational segmentation process was performed upon the immunogold-treated 40 μm tissue's reconstruction. First, the image stack was binarized using Fiji's image thresholding tool. After this, some graininess was still present within the image stack. To clean the images, a custom MATLAB script was written. This script ran a two-dimensional fast Fourier transform on each image, used the resulting power spectrum to remove noise from the images, inverse transformed the images, and then ran another thresholding process. In this way, the graininess was removed from each image slice within the reconstruction. It should be noted that this preprocessing method might not be as effective for some other x-ray microscopy datasets since variations in the characteristics of images may necessitate different treatments. After these steps, Vaa3D's APP2 plugin (Xiao & Peng, 2013) was employed to trace the neurites of the thresholded and cleaned reconstruction. The resulting segmentation demonstrates strong correspondence to the features seen in the raw imaging data (Fig. 4A). For instance, the MSN and the long filaments that were speculated to be axons are visible in the segmented reconstruction (Fig. 4B). The segmentation does exhibit inaccuracies regarding the fine details of the neurites, especially within the denser regions of the dataset. However, a more pressing issue is that the numerous neuronal structures are represented as a single fused aggregate within the segmented reconstruction. As such, it would be prudent to investigate strategies for automatic or manual editing of the segmentation to further refine the result. Despite these issues, the segmented reconstruction represents a promising first step in the analysis of this type of x-ray microscopy imaging dataset.

Next, 5 nm spherical gold nanoparticles were conjugated to anti-D1R antibodies. These nanoparticles were employed to treat an ~1 mm^3 tissue volume from rat striatum (with a 1:4

dilution from stock). The reason for using these smaller immunogold constructs was to increase penetration into the large tissue volume. After staining this tissue and packaging it into a 1 mm diameter plastic tube, a three-dimensional reconstruction was acquired using the ZEISS Xradia 520 Versa XRM. This scan took 16h (2,801 projections) with an ~0.8 mm^3 FOV using the XRM's 20x lens. In the resulting reconstruction, some neuronal processes were visible, though many regions were obscured by large clumps of material (Fig. 5A-C). This issue may have arisen due to the high concentration of nanoparticles used in an effort to further increase tissue penetration (a 1:4 dilution as compared to a 1:100 dilution in the previous experiment). As a consequence, it was difficult to computationally segment this dataset as was done with the 40 μm slices. Upon visual inspection, segmentations were largely inconsistent with the raw image data. Nonetheless, these data are promising since they indicate that large tissue volumes are potentially amenable to nanoparticle-based stains. With further improvement of the technique, large tissue volumes might be imaged with the same level of detail that was found in the sliced tissue.

Discussion

In this investigation, I demonstrate that gold nanoparticles with covalently linked antibodies are usable as a contrast agent for x-ray microscopic imaging of neuronal tissue. By employing standard immunohistochemical techniques, neurons expressing desired biomarkers can be stained with immunogold constructs and visualized using a laboratory XRM. To the best of my knowledge, this represents the first instance of an immunogold-based technique that is able to resolve individual neurites. Furthermore, past studies have generally utilized synchrotron sources instead of laboratory XRMs for absorption-based x-ray microtomography. Since only a few

synchrotron facilities exist, my results using a laboratory XRM may help advance the potential accessibility of x-ray microscopic imaging for neuroscience.

Based on my work with staining thick volumes, the primary limitation of nanoparticle-based x-ray contrast agents seems to arise from penetration of fixed tissue. However, future research may reveal ways to overcome this challenge. Decreasing the size of the immunogold constructs did allow some diffusion into the ~1 mm^3 volume, so further miniaturization may help improve tissue penetration. This might be achieved by conjugating monovalent Fab fragments, nanobodies, or other small non-antibody binding reagents (Bedford et al., 2017) to carboxylated gold nanoclusters with diameters of 1.5 nm or less. Since these materials are commercially available, they may facilitate construction of miniaturized immunogold particles with relative ease. In addition, tissue clearing methods such as iDISCO may help improve the permeability of fixed tissue (Marx, 2016; Renier et al., 2014). It may also be possible to inject immunogold into living animals prior to sacrifice and tissue fixation (Khongkow et al., 2019). Living tissue is substantially more permeable to nanoparticles than fixed tissue (Song et al., 2017), so this may enable better labeling of biomarkers with immunogold. To maximize biocompatibility and prevent immune responses from interfering with binding, the particles could be coated with polymer chains such as PEG or with lipid membranes (Khongkow et al., 2019). Using such methods, better staining of thick tissue volumes with immunogold particles might be achieved.

My eventual goal for using x-ray microscopy on brain tissue is to map both the structural morphologies of neurons and their synaptic connections. To facilitate these connectomics applications, immunogold particles with antibodies that target synaptic biomarkers such as neurexin or neuroligin and phosphomolybdic acid (PMA) could be used to co-stain tissue. PMA is a nonspecific chemical x-ray contrast agent that is very similar to phosphotungstic acid (PTA)

(Golding, Ponder, & Byrne, 2009; Metscher, 2009). As mentioned earlier, PTA has been used with great success in whole-body staining and x-ray microscopy of larval and juvenile zebrafish (Ding et al., 2019). But unlike PTA, PMA possesses a substantially different x-ray absorption coefficient compared to gold due to the greater difference between the Z-numbers of gold and molybdenum than between gold and tungsten. Because of this, two x-ray scans at each of the appropriate energies for gold and molybdenum absorption could facilitate imaging of both the locations of synapses and the general anatomy of the neurons within the tissue. By thresholding the "synapse only" scan and then overlaying the images, the synapses could be placed in the context of the rest of the neuronal anatomy. Synaptic connections between neurons would be identifiable without requiring the resolution of an electron microscope. As such, this method may allow x-ray microscopy to facilitate rapid connectomic mapping.

Developing expansion x-ray microscopy (ExxRM) may further improve the applicability of XRM-based method for connectomics. Performing tissue expansion would increase the effective resolution of an x-ray microscope by the expansion factor n. But the volume of the sample would increase by a factor of n^3. Rapid imaging of such large volumes could be carried out using a synchrotron radiation source. The acquisition times of synchrotron-based XRM for millimeter-scale FOVs range from a few minutes (Fonseca et al., 2018; R Mizutani et al., 2013) to just 20 seconds when using a polychromatic pink beam (Ding et al., 2019). The resolution of synchrotron-based XRM is often around 0.5-1.0 μm^3 (Ding et al., 2019; Fonseca et al., 2018; R Mizutani et al., 2013). With 4x tissue expansion, this resolution would increase to 125-250 nm^3. If the conditions from Ding et al.'s study (20 second acquisition time, 0.743 μm^3 resolution, and 1.5 mm^3 FOV) could be achieved with a 4x expanded Etruscan shrew brain, the entire brain might undergo

imaging at 186 nm^3 resolution in less than a day. Synchrotron-based ExxRM has enormous potential for mapping whole brains at subcellular resolution.

I show targeted staining of D1R within rat striatum using immunogold and subsequent three-dimensional imaging of the samples via XRM. This method should be widely applicable since any antibody could be covalently linked to gold nanoparticles and used to stain desired biomarkers. Although penetration of thick volumes has proven challenging, decreasing the size of the immunogold constructs and applying tissue clearing methods may help ameliorate this difficulty. Immunogold-based treatment may also be combined with non-specific contrast agents that exhibit distinct x-ray absorption coefficients. In this way, biomarkers could be imaged against the backdrop of their anatomical context. Tissue expansion may increase the effective resolution of XRM and so further enhance the quality of brain imaging data. The rapid scan times of synchrotron radiation sources may allow for efficient mapping of entire brains. My immunogold staining technique provides a starting point for developing a suite of XRM-based connectomics tools towards mapping brains in order to help develop superior computational models of neuronal tissue.

Methods

Conjugation of antibodies to gold nanoparticles

Carboxylated gold nanorods with dimensions of 60×27 nm and carboxylated spherical gold nanoparticles with 5 nm diameters were acquired from Cytodiagnostics. Anti-D1R antibodies were purchased from Abcam, 2-(N-morpholino)ethanesulfonic acid (MES) was obtained from Sigma Aldrich, and the N-hydroxysulfosuccinimide (Sulfo-NHS) and 1-Ethyl-3-(3-dimethylaminopropyl)carbodiimide hydrochloride (EDC) were acquired from Thermo Scientific. The protocol provided by Cytodiagnostics was used to conjugate the anti-D1R antibodies to gold

nanorods and spherical nanoparticles. Due to the small size of the spherical nanoparticles, the centrifugation steps of the protocol were carried out at 33,000 g using an ultracentrifuge. When performing the conjugation protocol with the larger nanorods, a tabletop centrifuge was used at 6,500 g instead.

Immunohistochemical treatments

PFA-fixed tissue slices of 40 μm thickness were prepared using a cryostat and stored in PBS prior to use. Three 10 minute washes in PBS with shaking were performed at room temperature before transferring the tissue to wells containing PBS with 0.2% Triton X-100 and 10% normal goat serum (NGS) and incubating for 2 h with shaking at room temperature. Next, the tissue was transferred to a well containing PBS with 0.2% Triton X-100, 2% NGS, and gold nanorods with conjugated anti-D1R antibodies (1:100 dilution from stock) and incubated with shaking at 4°C for two days. For the control slice, the tissue was transferred to a well containing PBS with 0.2% Triton X-100, 2% NGS, and unmodified gold nanorods and incubated with shaking at 4°C for two days. Three 10 minute washes in PBS with shaking were then performed at room temperature.

Slices were then moved to wells containing 0.2% Triton X-100 and Alexa Fluor® 488 Goat Anti-Rabbit antibodies (1:100 dilution from stock) and incubated with shaking at room temperature for 2 h. Three more 10 minute washes in PBS with shaking were performed at room temperature. The slices were transferred to wells containing PBS with 2% NeuroTrace 435/455 Blue Fluorescent Nissl Stain and incubated with shaking at room temperature for 1 h. Three final 10 minute washes in PBS with shaking were performed at room temperature. Prolong® Diamond was used to mount the tissue on slides and the slices were imaged using fluorescence microscopy.

PFA-fixed tissue volumes with dimensions of ~1 mm^3 were prepared using a brain matrix and stored in PBS prior to use. Three 10 minute washes in PBS with shaking were performed at room

temperature before transferring the tissue to a well containing PBS with 0.2% Triton X-100 and 10% NGS and incubating for 2 h with shaking at room temperature. The tissue was moved to a well containing PBS with 0.2% Triton X-100, 2% NGS, and 5 nm spherical gold nanoparticles with conjugated anti-D1R antibodies (1:4 dilution from stock) and incubated with shaking at 4°C for two days. Three more 10 minute washes in PBS with shaking were performed at room temperature. Due to their thickness, the tissue volumes were not imaged with fluorescence microscopy and instead were prepared for x-ray microscopy immediately after the last three washes.

X-ray microscopy

Prior to x-ray imaging, tissue samples were placed inside of plastic tubes with 2 mm diameters. The ends of the tubes were sealed using rubber plugs and superglue and then the sealed tubes were mounted on metal pins which fit into the x-ray microscope's sample holder. The ZEISS Xradia 520 Versa x-ray microscope was employed to facilitate three-dimensional imaging of the samples. This x-ray microscope's 0.4x and 4x lenses was used to decide how to position the sample relative to the detector in order to choose an appropriate FOV. Final images were acquired using the x-ray microscope's 20x lens. The scan of the tissue slice was carried out at 386 nm pixel size, took 13h to acquire, and used 3,000 projections. The scan of the tissue volume was carried out at 403 nm pixel size, took 16h to acquire, and used 2,801 projections.

Segmentation

The three-dimensional reconstructions of the tissue slice underwent computational segmentation using the following process. Preprocessing steps were performed upon each two-dimensional image within a stack of 1,923 images that comprised the three-dimensional imaging volume. First, Fiji's image thresholding tool facilitated binarization of the images. Then a custom

MATLAB script was utilized to further clean the images. After these preprocessing steps, running the APP2 plugin within Vaa3D on the three-dimensional image data enabled tracing and segmentation of the neurites.

Figures

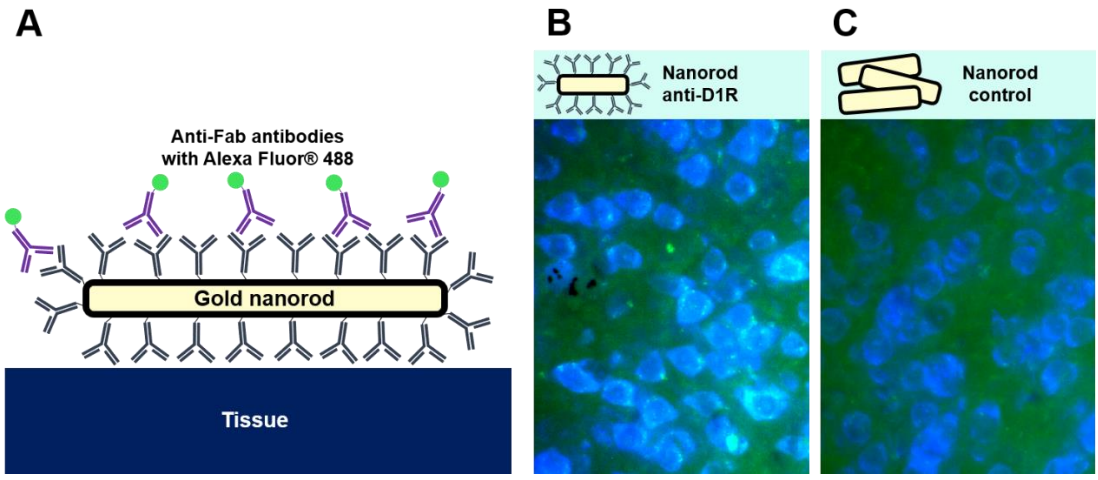

Figure 1 Validation of immunogold reactivity against D1R using fluorescence microscopy. **(A)** Immunogold constructs were detected using an anti-Fab secondary antibody with an Alexa Fluor® 488 fluorophore. **(B)** Striatum treated with nanorods linked to antibodies demonstrated membrane-localized fluorescence. **(C)** Striatum treated with unmodified nanorods did not show fluorescence.

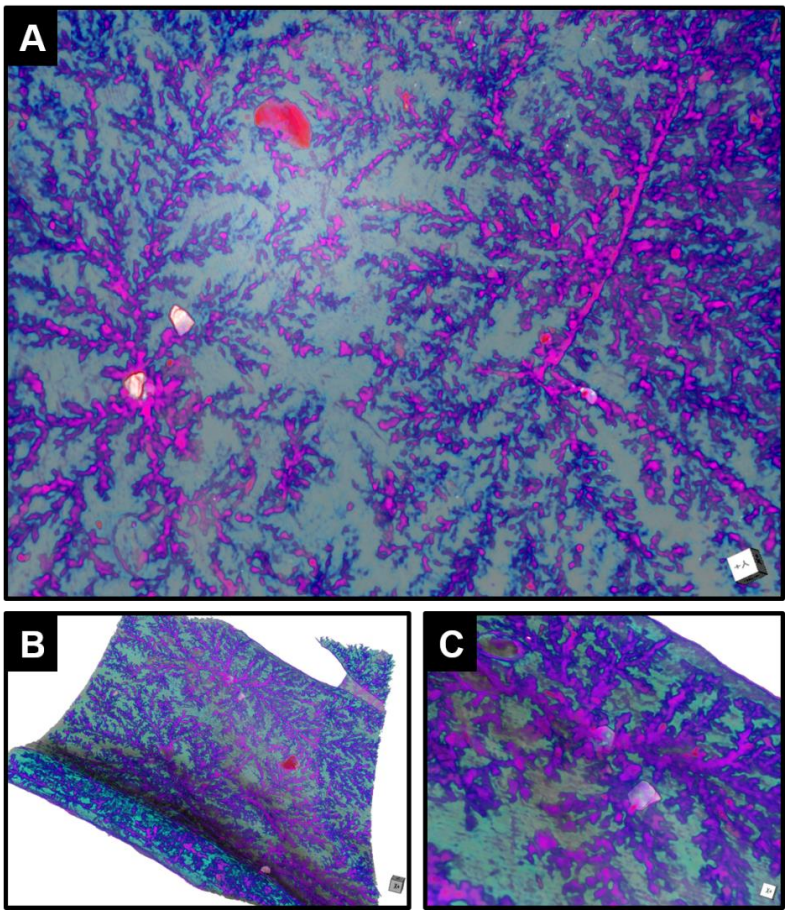

Figure 2 Three-dimensional reconstruction of an ~700 μm^3 volume containing a slice of rat striatum. The tissue was treated with 60×27 nm gold nanorods covalently linked to anti-D1R antibodies. **(A)** View perpendicular to the face of the slice. On the left side of the image, a MSN is visible. At the right side of the image, there are two long filaments that might be axons. **(B)** Perspective view of the reconstructed region. **(C)** Zoomed perspective view of the MSN. The globular extensions on the dendrites are likely dendritic spines. These images were generated using the Dragonfly software.

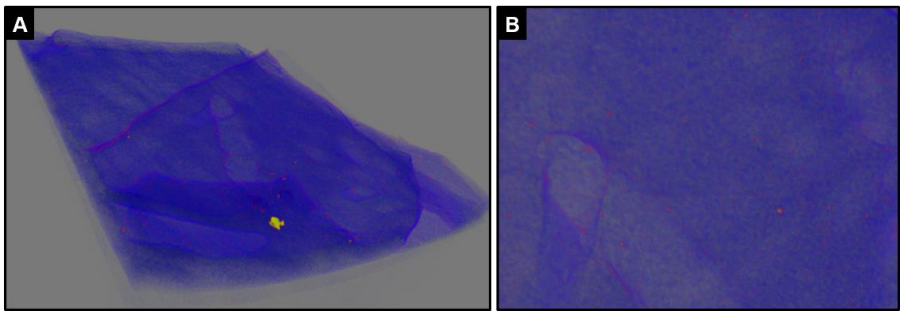

Figure 3 Three-dimensional reconstruction of an ~700 μm^3 volume containing a slice of rat striatum. The tissue was treated with 60×27 nm unmodified gold nanorods. **(A)** Perspective and **(B)** zoomed views of the reconstructed region do not reveal any distinguishable morphological features.

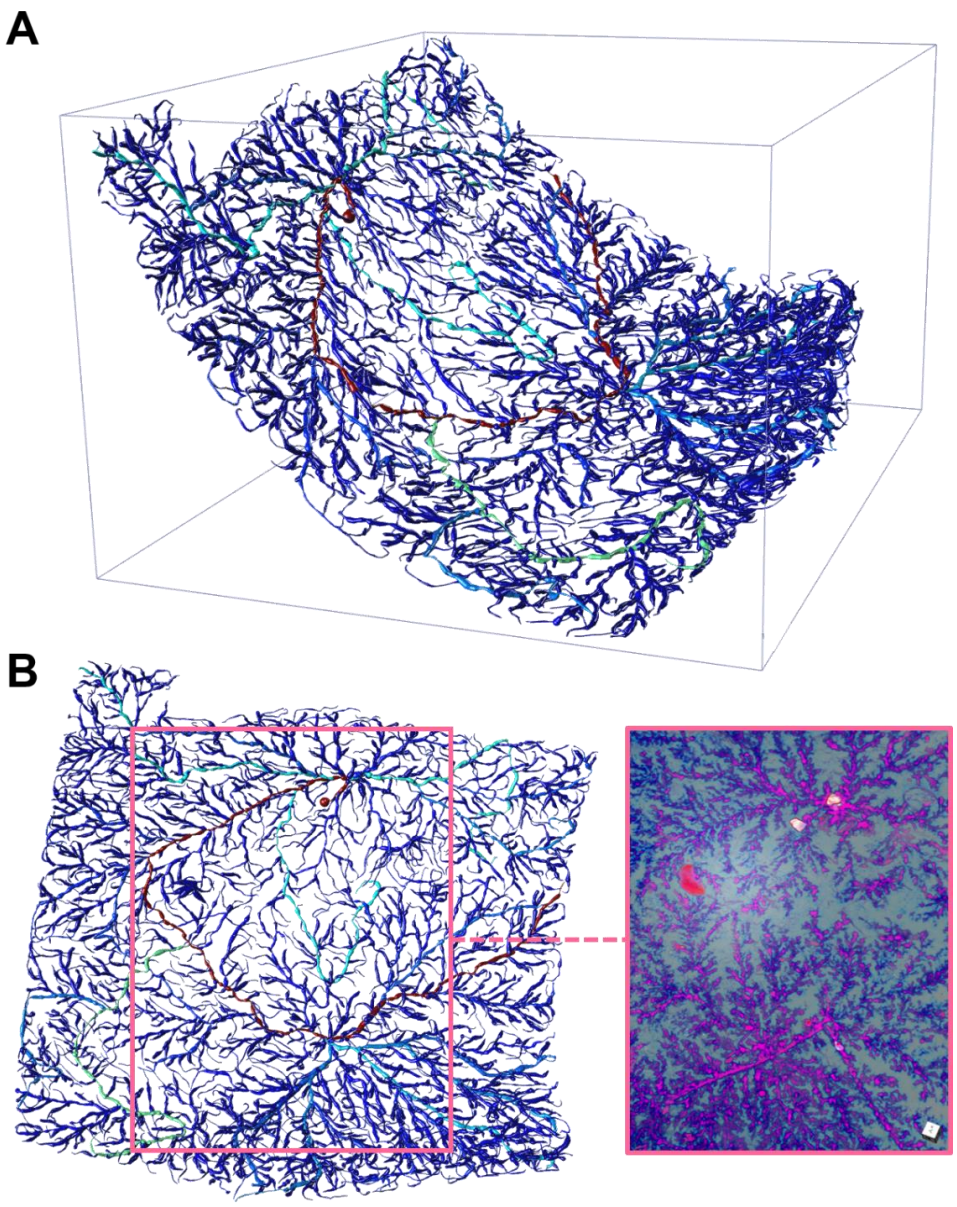

Figure 4 Segmentation of immunogold-treated tissue slice reconstruction. **(A)** Perspective view of segmentation as visualized using Vaa3D. **(B)** View of segmentation perpendicular to the face of the slice as visualized using Vaa3D along with a comparison to the raw image data. A MSN and possible axonal filaments are visible in both the segmentation and the raw image data.

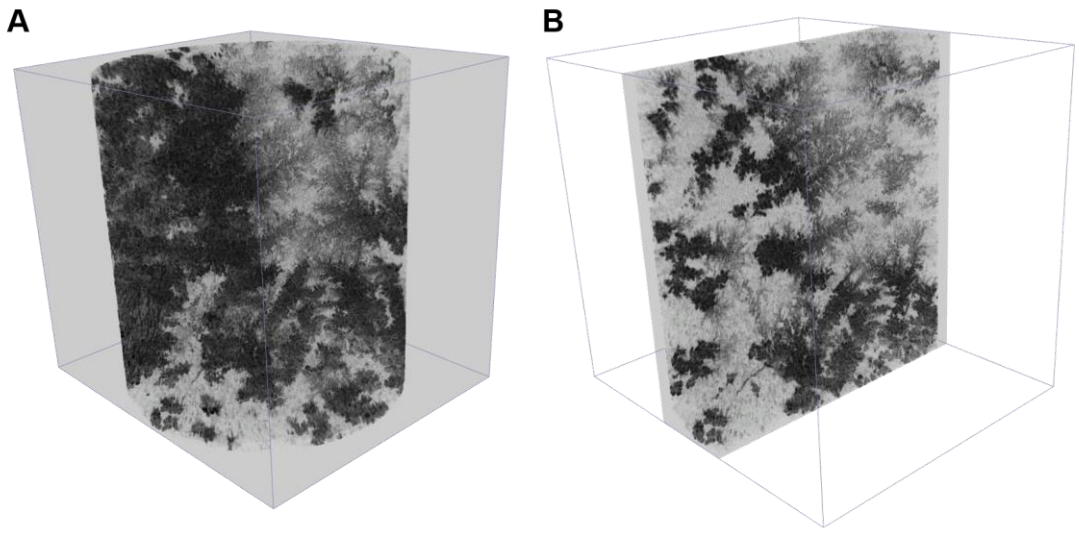

Figure 5 Three-dimensional reconstruction of an ~800 μm^3 volume of tissue from rat striatum. The tissue was treated with 5 nm spherical gold nanoparticles covalently linked to anti-D1R antibodies. **(A)** The entire three-dimensional volume as visualized using Vaa3D. **(B)** Cross section of the three-dimensional volume as visualized using Vaa3D. Note that some branching filamentous structures are visible, but that it is difficult to distinguish them in many areas due to the high staining density. These areas of high density likely arose from the high concentration of nanoparticles used to maximize tissue penetration.

References

Arkhipov, A., Gouwens, N. W., Billeh, Y. N., Gratiy, S., Iyer, R., Wei, Z., … Koch, C. (2018). Visual physiology of the layer 4 cortical circuit in silico. *PLOS Computational Biology*, *14*(11), e1006535. Retrieved from https://doi.org/10.1371/journal.pcbi.1006535

Bedford, R., Tiede, C., Hughes, R., Curd, A., McPherson, M. J., Peckham, M., & Tomlinson, D. C. (2017). Alternative reagents to antibodies in imaging applications. *Biophysical Reviews*, *9*(4), 299–308. https://doi.org/10.1007/s12551-017-0278-2

Bezaire, M. J., Raikov, I., Burk, K., Vyas, D., & Soltesz, I. (2016). Interneuronal mechanisms of hippocampal theta oscillations in a full-scale model of the rodent CA1 circuit. *ELife*, *5*, e18566. https://doi.org/10.7554/eLife.18566

Chen, B., Legant, W. R., Wang, K., Shao, L., Milkie, D. E., Davidson, M. W., … Betzig, E. (2014). Lattice light-sheet microscopy: Imaging molecules to embryos at high spatiotemporal resolution. *Science*, *346*(6208). Retrieved from http://science.sciencemag.org/content/346/6208/1257998.abstract

Chen, F., Tillberg, P. W., & Boyden, E. S. (2015). Expansion microscopy. *Science*, *347*(6221), 543 LP-548. https://doi.org/10.1126/science.1260088

Ding, Y., Vanselow, D. J., Yakovlev, M. A., Katz, S. R., Lin, A. Y., Clark, D. P., … Cheng, K. C. (2019). Computational 3D histological phenotyping of whole zebrafish by X-ray histotomography. *ELife*, *8*, e44898. https://doi.org/10.7554/eLife.44898

Du, H., Hou, P., Zhang, W., & Li, Q. (2018). Advances in CLARITY-based tissue clearing and imaging. *Experimental and Therapeutic Medicine*, *16*(3), 1567–1576. https://doi.org/doi.org/10.3892/etm.2018.6374

Egger, R., Dercksen, V. J., Udvary, D., Hege, H.-C., & Oberlaender, M. (2014). Generation of dense statistical connectomes from sparse morphological data. *Frontiers in Neuroanatomy*. Retrieved from https://www.frontiersin.org/article/10.3389/fnana.2014.00129

Einevoll, G. T., Destexhe, A., Diesmann, M., Grün, S., Jirsa, V., de Kamps, M., … Schürmann, F. (2019). The Scientific Case for Brain Simulations. *Neuron*, *102*(4), 735–744. https://doi.org/https://doi.org/10.1016/j.neuron.2019.03.027

Fonseca, M. de C., Araujo, B. H. S., Dias, C. S. B., Archilha, N. L., Neto, D. P. A., Cavalheiro,

E., … Franchini, K. G. (2018). High-resolution synchrotron-based X-ray microtomography as a tool to unveil the three-dimensional neuronal architecture of the brain. *Scientific Reports*, *8*(1), 12074. https://doi.org/10.1038/s41598-018-30501-x

Gao, R., Asano, S. M., Upadhyayula, S., Pisarev, I., Milkie, D. E., Liu, T.-L., … Betzig, E. (2019). Cortical column and whole-brain imaging with molecular contrast and nanoscale resolution. *Science*, *363*(6424), eaau8302. https://doi.org/10.1126/science.aau8302

Golding, R. E., Ponder, W. F., & Byrne, M. (2009). Three-dimensional reconstruction of the odontophoral cartilages of Caenogastropoda (Mollusca: Gastropoda) using micro-CT: Morphology and phylogenetic significance. *Journal of Morphology*, *270*(5), 558–587. https://doi.org/10.1002/jmor.10699

Hwu, Y., Margaritondo, G., & Chiang, A.-S. (2017). Q&A: Why use synchrotron x-ray tomography for multi-scale connectome mapping? *BMC Biology*, *15*(1), 122. https://doi.org/10.1186/s12915-017-0461-8

Ke, M.-T., Nakai, Y., Fujimoto, S., Takayama, R., Yoshida, S., Kitajima, T. S., … Imai, T. (2016). Super-Resolution Mapping of Neuronal Circuitry With an Index-Optimized Clearing Agent. *Cell Reports*, *14*(11), 2718–2732. https://doi.org/https://doi.org/10.1016/j.celrep.2016.02.057

Khongkow, M., Yata, T., Boonrungsiman, S., Ruktanonchai, U. R., Graham, D., & Namdee, K. (2019). Surface modification of gold nanoparticles with neuron-targeted exosome for enhanced blood–brain barrier penetration. *Scientific Reports*, *9*(1), 8278. https://doi.org/10.1038/s41598-019-44569-6

Markram, H. (2006). The Blue Brain Project. *Nature Reviews Neuroscience*, *7*, 153. Retrieved

from http://dx.doi.org/10.1038/nrn1848

Markram, H., Muller, E., Ramaswamy, S., Reimann, M. W., Abdellah, M., Sanchez, C. A., … Schürmann, F. (2015). Reconstruction and Simulation of Neocortical Microcircuitry. *Cell*, *163*(2), 456–492. https://doi.org/10.1016/j.cell.2015.09.029

Marx, V. (2016). Optimizing probes to image cleared tissue. *Nature Methods*, *13*, 205. Retrieved from https://doi.org/10.1038/nmeth.3774

Matamales, M., Bertran-Gonzalez, J., Salomon, L., Degos, B., Deniau, J.-M., Valjent, E., … Girault, J.-A. (2009). Striatal Medium-Sized Spiny Neurons: Identification by Nuclear Staining and Study of Neuronal Subpopulations in BAC Transgenic Mice. *PLOS ONE*, *4*(3), e4770. Retrieved from https://doi.org/10.1371/journal.pone.0004770

Metscher, B. D. (2009). MicroCT for comparative morphology: simple staining methods allow high-contrast 3D imaging of diverse non-mineralized animal tissues. *BMC Physiology*, *9*(1), 11. https://doi.org/10.1186/1472-6793-9-11

Mizutani, R., Saiga, R., Ohtsuka, M., Miura, H., Hoshino, M., Takeuchi, A., & Uesugi, K. (2016). Three-dimensional X-ray visualization of axonal tracts in mouse brain hemisphere. *Scientific Reports*, *6*, 35061. Retrieved from http://dx.doi.org/10.1038/srep35061

Mizutani, R., Saiga, R., Takeuchi, A., Uesugi, K., & Suzuki, Y. (2013). Three-dimensional network of Drosophila brain hemisphere. *Journal of Structural Biology*, *184*(2), 271–279. https://doi.org/https://doi.org/10.1016/j.jsb.2013.08.012

Mizutani, R., & Suzuki, Y. (2012). X-ray microtomography in biology. *Micron*, *43*(2), 104–115. https://doi.org/https://doi.org/10.1016/j.micron.2011.10.002

Mizutani, R., Takeuchi, A., Akamatsu, G., Uesugi, K., & Suzuki, Y. (2008). Element-specific

microtomographic imaging of Drosophila brain stained with high-Z probes. *Journal of Synchrotron Radiation*, *15*. https://doi.org/10.1107/S0909049508003725

Mizutani, R., Takeuchi, A., Uesugi, K., Takekoshi, S., Nakamura, N., & Suzuki, Y. (2011). Building Human Brain Network in 3D Coefficient Map Determined by X-ray Microtomography. *AIP Conference Proceedings*, *1365*(1), 403–406. https://doi.org/10.1063/1.3625388

Novère, N. L. (2012). *Computational Systems Neurobiology*. Springer Netherlands.

Oberlaender, M., de Kock, C. P. J., Bruno, R. M., Ramirez, A., Meyer, H. S., Dercksen, V. J., … Sakmann, B. (2011). Cell Type–Specific Three-Dimensional Structure of Thalamocortical Circuits in a Column of Rat Vibrissal Cortex. *Cerebral Cortex*, *22*(10), 2375–2391. https://doi.org/10.1093/cercor/bhr317

Power, R. M., & Huisken, J. (2017). A guide to light-sheet fluorescence microscopy for multiscale imaging. *Nature Methods*, *14*, 360. Retrieved from https://doi.org/10.1038/nmeth.4224

Qi, Y., Yu, T., Xu, J., Wan, P., Ma, Y., Zhu, J., … Zhu, D. (2019). FDISCO: Advanced solvent-based clearing method for imaging whole organs. *Science Advances*, *5*(1), eaau8355. https://doi.org/10.1126/sciadv.aau8355

Renier, N., Wu, Z., Simon, D. J., Yang, J., Ariel, P., & Tessier-Lavigne, M. (2014). iDISCO: A Simple, Rapid Method to Immunolabel Large Tissue Samples for Volume Imaging. *Cell*, *159*(4), 896–910. https://doi.org/10.1016/j.cell.2014.10.010

Schalek, R., Lee, D., Kasthuri, N., Peleg, A., Jones, T., Kaynig, V., … Lichtman, J. W. (2016). Imaging a 1 mm3 Volume of Rat Cortex Using a MultiBeam SEM. *Microscopy and*

Microanalysis, *22*(S3), 582–583. https://doi.org/DOI: 10.1017/S1431927616003767

Song, E., Gaudin, A., King, A. R., Seo, Y.-E., Suh, H.-W., Deng, Y., … Saltzman, W. M. (2017). Surface chemistry governs cellular tropism of nanoparticles in the brain. *Nature Communications*, *8*, 15322. Retrieved from https://doi.org/10.1038/ncomms15322

Surmeier, D. J., Ding, J., Day, M., Wang, Z., & Shen, W. (2007). D1 and D2 dopamine-receptor modulation of striatal glutamatergic signaling in striatal medium spiny neurons. *Trends in Neurosciences*, *30*(5), 228–235. https://doi.org/https://doi.org/10.1016/j.tins.2007.03.008

Takemura, S., Aso, Y., Hige, T., Wong, A., Lu, Z., Xu, C. S., … Scheffer, L. K. (2017). A connectome of a learning and memory center in the adult Drosophila brain. *ELife*, *6*, e26975. https://doi.org/10.7554/eLife.26975

Wanner, A. A., Kirschmann, M. A., & Genoud, C. (2015). Challenges of microtome-based serial block-face scanning electron microscopy in neuroscience. *Journal of Microscopy*, *259*(2), 137–142. https://doi.org/10.1111/jmi.12244

Xiao, H., & Peng, H. (2013). APP2: automatic tracing of 3D neuron morphology based on hierarchical pruning of a gray-weighted image distance-tree. *Bioinformatics*, *29*(11), 1448–1454. https://doi.org/10.1093/bioinformatics/btt170